Leveraging Ligand Conjugation to Improve Luminescence Thermometry in Dy-Single-Molecule Magnets

Shraoshee Shome,[a] Naresh Chandra Maurya,[b] Moubani Mukherjee,[a] K. V. Adarsh,[b] Sanjit Konar*[a]

Contents:

S1. Experimental Section and Characterisations

Materials

All the reagents are commercially available and used without further purification. All chemicals are purchased from Sigma Aldrich Pvt. Ltd. Solvents were used as received.

Physical Measurements

IR spectra were recorded for all the samples with a Spectrum two spectrometer (PerkinElmer Inc.) in attenuated-total-reflectance (ATR) mode under ambient conditions. Spectra were recorded at 4 cm^{-1} resolution with a wavelength range of 4000-400 cm^{-1}. Elemental analyses (CHNS) were performed at the Elementar Micro Vario Cube elemental analyzer.

Powder XRD for all the samples was carried out in the PANalytical EMPYREAN instrument using Cu Kα radiation. PerkinElmer TGA 4000 thermogravimetric analyzer was used for the thermodynamic analysis of all the samples with an alumina sample holder and an N_2 flow of 10 mL per minute, the analysis was carried out between 25 °C to 600 °C at a heating rate of 5 °C per minute.

Single Crystal X-ray diffraction

The block-shaped pale yellow single crystals were mounted on a cryo-loop with paratone-N oil on a Brüker D8 Venture diffractometer, and graphite-monochromated Mo K*α* radiation (λ = 0.71073 Å) was used to capture the diffraction data of single crystals at low temperature 100 K for complex 1Np and 1Ph. The APEX-5 crystallographic software was used for data processing, integration, and scaling. XPREP software was employed for space-group determination. Data from all of the complexes were gathered utilizing using ϕ and ω scans. All of the structures were solved using intrinsic phasing with the SHELXT[1] structure solution and refinement with SHELXL utilizing *Olex2*[2] as the graphical interface. The models were improved with SHELXL and complete matrix least-squares minimization on F2.[3] All non-H atoms underwent anisotropic refinement. The riding model was used to improve the geometric placement and arrangement of the complex's H atoms. SHELXL-97 and Olex2 were used to do the computations. Both the whole SHELX model and the complete reflection data are included in the files that were submitted.

Magnetic Measurement

Magnetic measurements were performed using a Quantum Design SQUID-VSM (MPMS) magnetometer. The measured values were corrected for the experimentally measured contribution of the sample holder, while the derived susceptibilities were corrected for the diamagnetic contribution of the sample, estimated from Pascal's tables. The variable temperature magnetic susceptibility of all the complexes was collected in a DC field of 1000 Oe in the temperature range of 2-300 K.

Photophysical Measurements

All the photophysical measurements are performed on a solid crushed sample in the form of a pellet. Photoluminescence (PL) and photoexcitation (PLE) spectra were collected using the Fluorolog Horiba PL spectrophotometer using Xenon lamp excitation. For temperature-dependent PL measurements, the sample pallet has been attached to a glass slide using Poly(methyl methacrylate) (PMMA) and mounted on a sample holder attached to a closed cycle He cryostat (Advanced Research Systems) with a temperature controller (Lake Shore Cryotronics) to achieve the desired lower temperatures. Equations S1, S2, and S3 are used to calculate the thermometric parameter (Δ), relative thermal sensitivity (S_r), and temperature uncertainty (δT) respectively. The Δ *vs* T plot was fitted using equation S4.

$$\Delta = \frac{I_2}{I_1} \quad \textbf{Equation S1}$$

$$S_r = \frac{1}{\Delta}\left(\frac{\delta\Delta}{\delta T}\right) \quad \textbf{Equation S2}$$

$$\delta T = \frac{1}{S_r}\left(\frac{\delta\Delta}{\Delta}\right) \quad \textbf{Equation S3}$$

$$\Delta = A_2 + \frac{A_1 - A_2}{1 + \left(\frac{T}{T_0}\right)^p} \quad \textbf{Equation S4}$$

Delta Flex-01-DD/HORIBA time-correlated single photon counting (TCSPC) setup was used for time-resolved measurements. The fitting of the excited state lifetime decay was done using the following multi-exponential equation:

$$I(t) = \sum_i \alpha_i e^{-t/\tau_i} \quad \textbf{Equation S5}$$

Where α_i is the amplitude of the i^{th} component having lifetime τ_i. The average lifetime $<\tau>$ is given by:

$$<\tau> = \frac{\sum_i \alpha_i \tau_i}{\sum_i \alpha_i} \quad \textbf{Equation S6}$$

Syntheses of Complexes

Synthesis of $[Dy_2(L_{Np})_6(BPYM)]$ (Complex 1Np)

The reaction of aqueous 4,4,4-trifluoro-1-(2-naphthyl)-1,3-butanedione (0.3 mmol), and sodium hydroxide (0.3 mmol) solution with aqueous $DyCl_3.6H_2O$ (0.1 mmol) produced a white precipitate. The precipitate was filtered and vacuum-dried. Now 0.1 mmol of the white ppt is dissolved in 5 ml dichloromethane and to this 0.05 mmol of 4,4'-bypyrimidine (bpym) is added. The reaction mixture is stirred for 6 hours at room temperature and then filtered and kept for slow evaporation. After almost 3-4 days very pale yellow block-shaped crystals start to form. The crystals are filtered and washed with 5 ml cold diethyl ether. Yield: ~90%, Elemental analysis Calculated for $C_{92}H_{54}Dy_2F_{18}N_4O_{12}$ (1Np): C: 53.27, H: 2.62, N: 2.70. Found: C: 53.50, H: 2.59, N: 2.66.

Synthesis of $[Dy_2(L_{Ph})_6(BPYM)]$ (Complex 1Ph)

Complex 1Ph was synthesized as per the reported procedure and the pale yellow block-shaped crystals were obtained.[4] Yield: ~95%, Elemental analysis Calculated for $C_{68}H_{42}Dy_2F_{18}N_4O_{12}$ (1Ph): C: 46.04, H: 2.39, N: 3.16. Found: C: 46.01, H: 2.42, N: 3.25.

S2. Single crystal X-ray diffraction

Table S1. Crystal data and structure refinement parameters for complexe 1Np.

Empirical formula	**$C_{92}H_{54}Dy_2F_{18}N_4O_{12}$ (CCDC N0. 2395423)**
Formula weight	**2074.39**
Temperature/K	**140.00**
Crystal system	**Triclinic**
Space group	***P$\bar{1}$***
a/Å	**10.133(2)**
b/Å	**12.501(3)**
c/Å	**17.148(3)**
α/°	**105.694(6)**
β/°	**97.862(5)**
γ/°	**101.469(6)**
Volume/Å^3	**2007.3(7)**
Z	**1**
ρ_{calc} g/cm^3	**1.716**
μ/mm-1	**1.957**
F(000)	**1024.0**
Crystal size/mm^3	**0.15 × 0.12 × 0.10**
Radiation	**MoK_α (λ = 0.71073)**
2Θ range for data collection/°	**4.188 to 50.41**

Index ranges	**-12 ≤ h ≤ 12, -14 ≤ k ≤ 14, -20 ≤ l ≤ 19**
Reflections collected	**22769**
Independent reflections	**7118 [R_{int} = 0.0580, R_{sigma} = 0.0701]**
Data/restraints/parameters	**7118/0/577**
Goodness-of-fit on F2	**1.024**
Final R indexes [I>=2σ (I)]	**R1 = 0.0442, wR2 = 0.0973**
Final R indexes [all data]	**R_1 = 0.0616, wR_2 = 0.1060**
Largest diff. peak/hole / e Å^{-3}	**2.10/-1.16**

S3. Shape analysis

a)

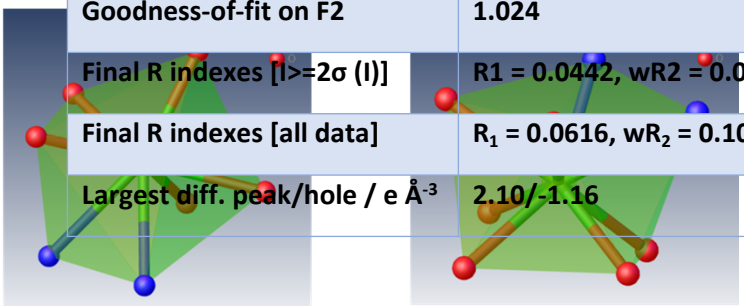

Figure S1: Polyhedral view of a) 1Np and b) 1Ph.

Table S2: Shape analysis of complex 1Np and 1Ph.

Structure	Point Group	Distortion (Dy) Complex 1Np	Distortion (Dy) Complex 1Ph
Octagon (**OP-8**)	D_{8h}	31.799	30.318
Heptagonal pyramid (**HPY-8**)	C_{7v}	23.167	23.214
Hexagonal bipyramidal (**HBPY-8**)	D_{6h}	15.700	16.638
Cube (**CU-8**)	O_h	9.069	10.339
Square antiprism (**SAPR-8**)	D_{4d}	1.791	**0.950**
Triangular dodecahedron (**TDD-8**)	D_{2d}	**0.496**	1.316
Johnson gyrobifastigium J26 (**JGBF-8**)	D_{2d}	14.752	14.606
Johnson elongated triangular bipyramid J14 (**JETBPY-8**)	D_{3h}	29.572	28.036

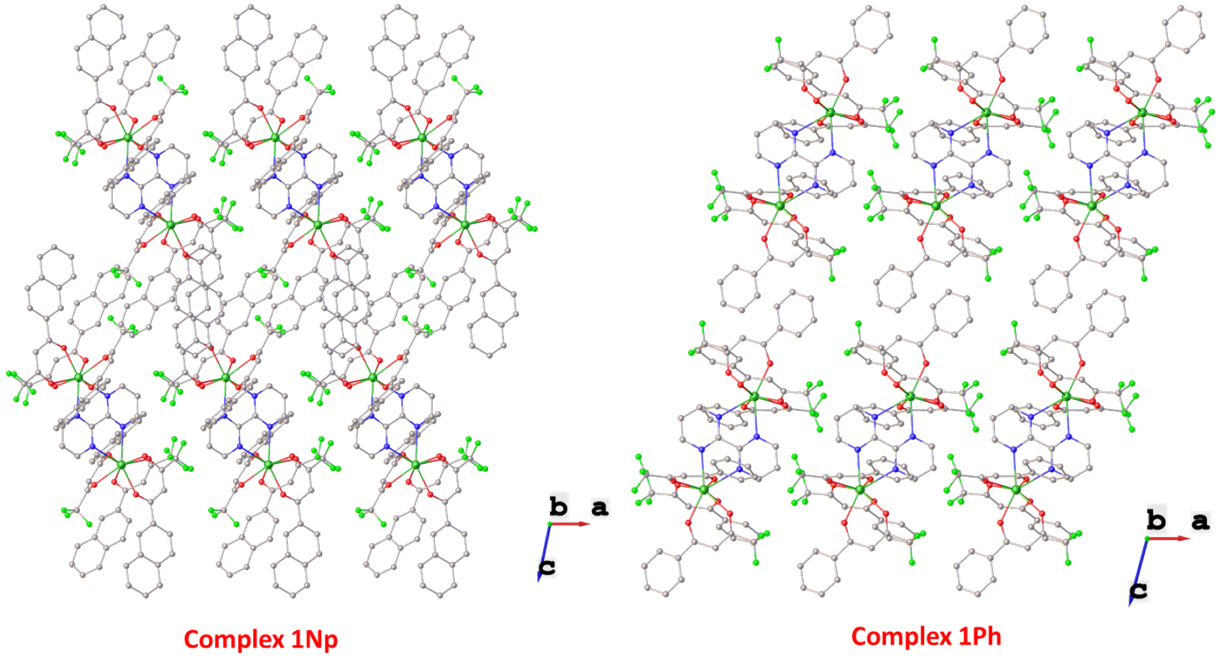

Figure S2: Packing diagram of complex 1Np and 1Ph along crystallographic b-axis.

S4. IR spectroscopy

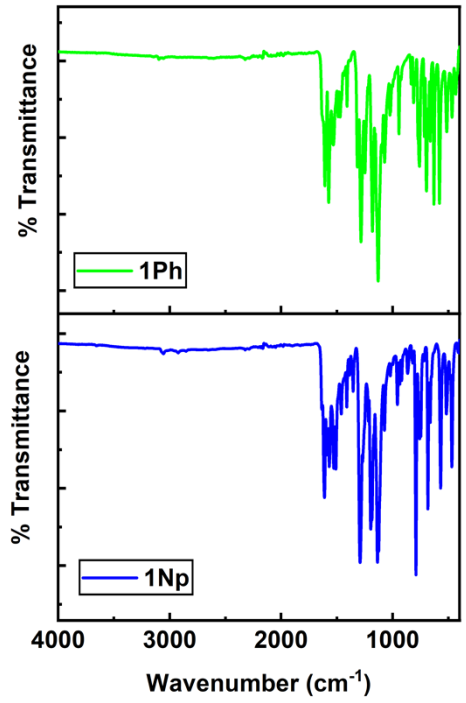

Figure S3: IR spectrum of complex 1Np and 1Ph.

S5. Powder X-ray diffraction analysis

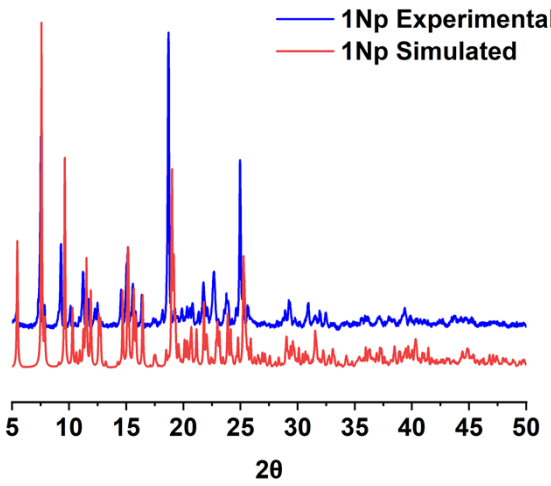

Figure S4: Powder X-ray diffraction pattern of complex 1Np. The similar pattern in experimental and simulated data (obtained from crystal structure) confirms the structural integrity of the complex in powder form.

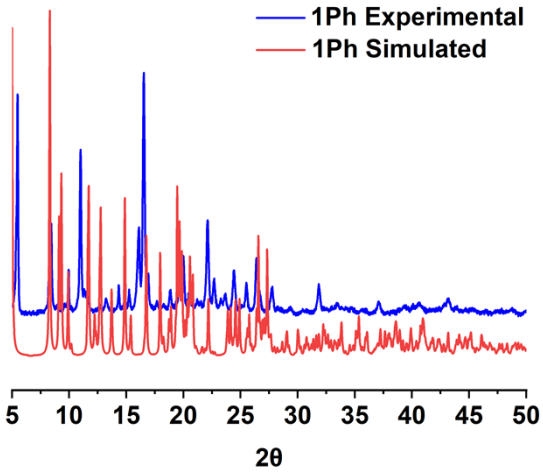

Figure S5: Powder X-ray diffraction pattern of complex 1Ph. The similar pattern in experimental and simulated data (obtained from crystal structure) confirms the structural integrity of the complex in powder form.

S6. Thermogravimetric analysis

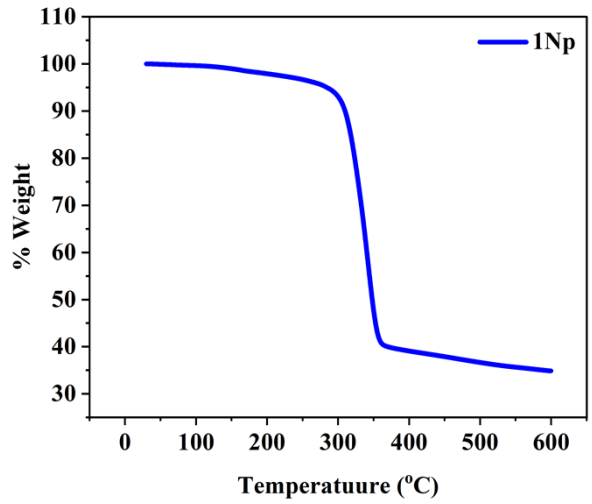

Figure S6: TGA plot of complex 1Np.

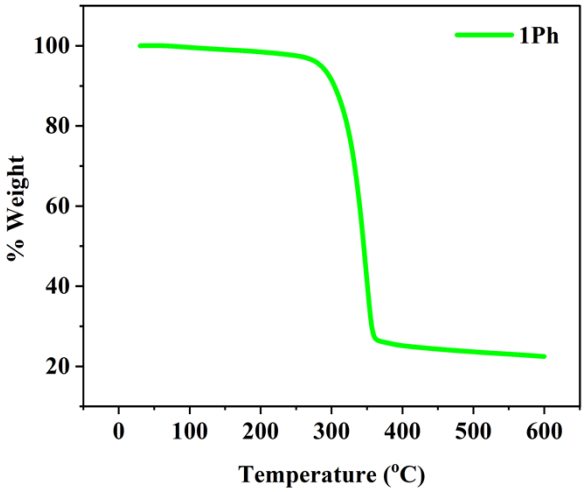

Figure S7: TGA plot of complex 1Ph.

S7. Magnetic Analysis

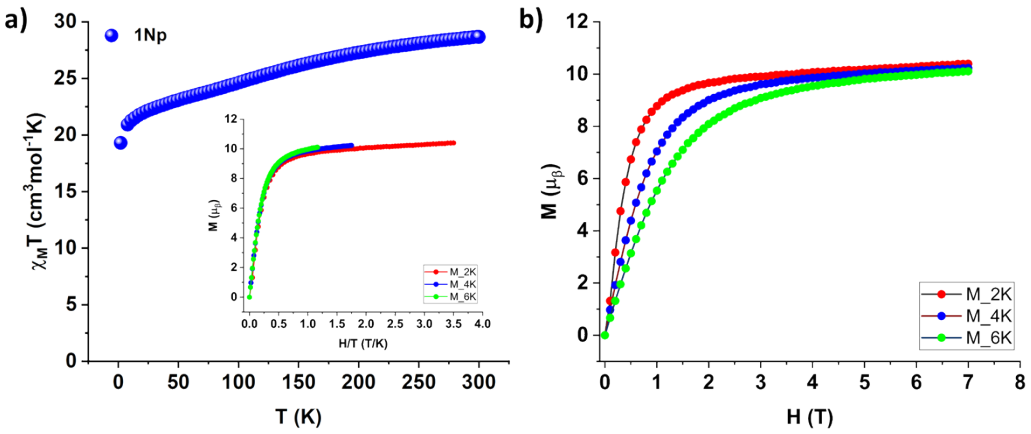

Figure S8: (a) The DC magnetic susceptibility measurement of 1Np in the 2-300 K temperature range (Inset: Reduced magnetization plot of 1Np). (b) The field dependence of magnetization of complex 1Np.

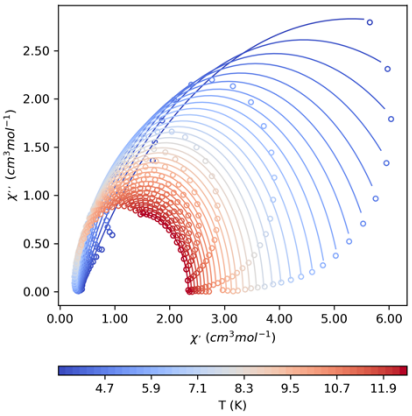

Figure S9. The cole-Cole plot of 1Np from CC-FIT2 using Orbach and Raman relaxation processes.

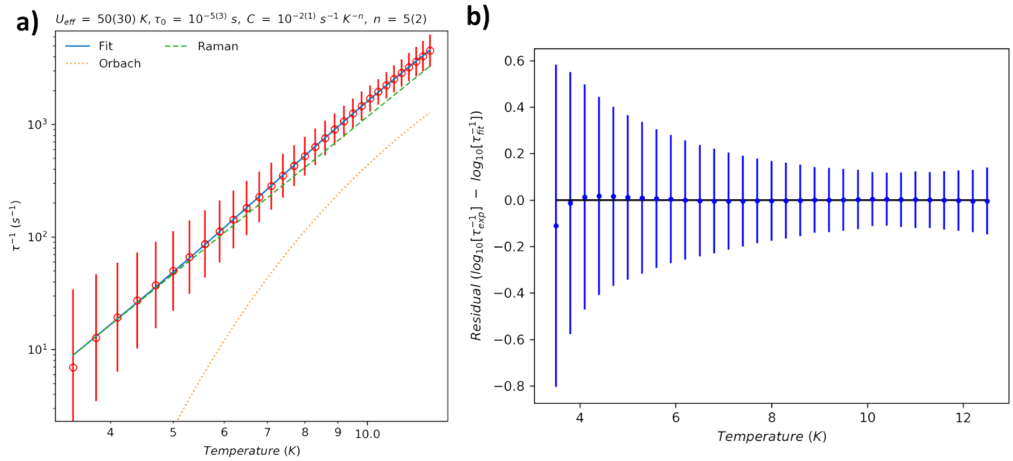

Figure S10. a) Fitting, and b) residuals of relaxation time vs. temperature considering Orbach and Raman relaxation in CC-FIT2 for 1Np. The equation used for fitting is $\tau^{-1} = \tau_0^{-1}\exp(-U_{eff}/k_BT) + CT^n$.

S8. Photophysical Analysis

Table S3: The fitting parameters obtained using a logistic function (Equation S4)[5] to describe the dependence of the ratiometric thermometric parameter Δ on temperature for complex 1Np.

Parameter	1Np	1Ph
A_1	23.12373 ± 0.46748	19.4873 ± 0.47618
A_2	1.30979 ± 0.36629	0.09599 ± 0.84277
T_0/K	53.74536 ± 1.7851	86.85996 ± 5.03497
p	1.90797 ± 0.12936	1.64102 ± 0.16427

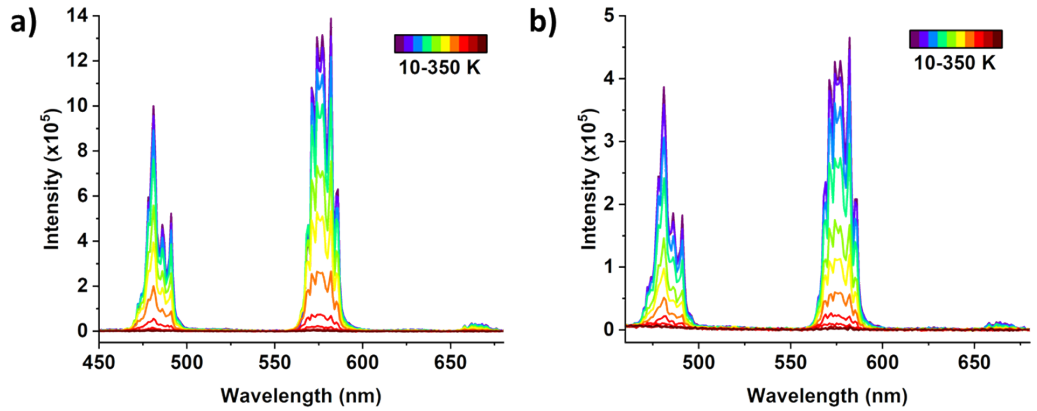

Figure S11: a) The emission spectrum of complex 1Np (PL,λ_{exc} = 380 nm) and b) 1Ph (PL,λ_{exc} = 360 nm) at 10 K. The complex 1Np shows a very high emission intensity compared to 1Ph.

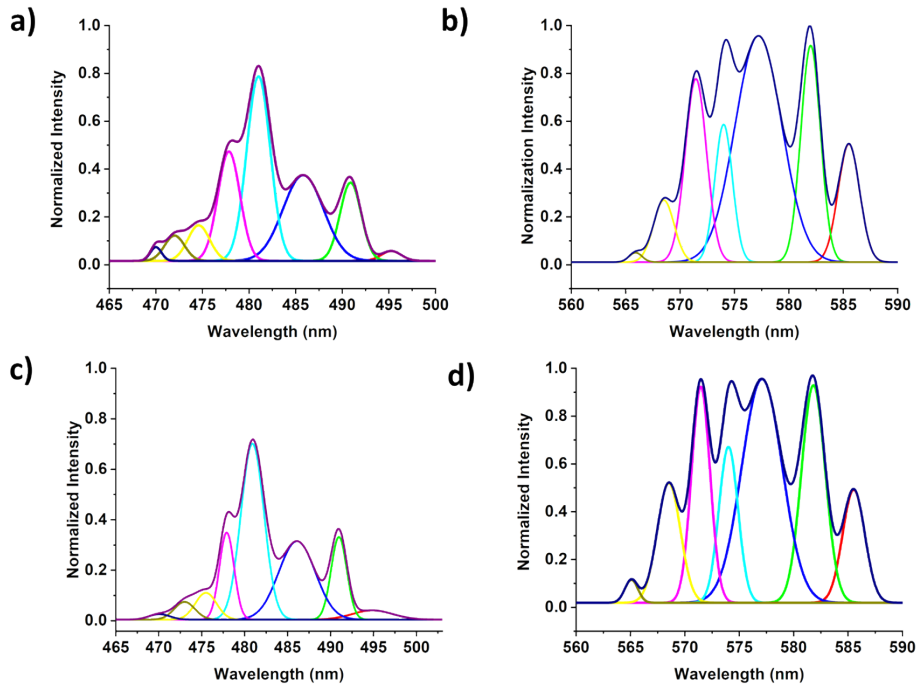

Figure S12: a) High-resolution normalized emission spectra at 10 K showing the m_J components of $^6H_{15/2}$ and b) $^6H_{13/2}$ levels of Dy (III) in 1Np. c) High-resolution normalized emission spectra at 10 K showing the m_J components of $^6H_{15/2}$ and d) $^6H_{13/2}$ levels of Dy (III) in 1Ph.

Table S4: The fitting parameters and average lifetime obtained using a bi-exponential function in fitting the lifetime decay for complex 1Np and 1Ph.

Complex	τ_1	α_1	τ_2	α_2	$<\tau>$	χ^2
1Np	0.59 ns	0.70	5.04 ns	0.30	1.92 ns	0.95
1Ph	0.53 ns	0.28	7.47 ns	0.72	5.53 ns	0.95

Table S5: A comparative table of magnetic and photophysical parameters for complexes 1Np and 1Ph.

PARAMETERS	1Np	1Ph
Operating temperature range	10-300 K	10-300 K
Maximum relative sensitivity (S_{max})	1.60 % K^{-1}	0.97 % K^{-1}
Temperature of S_{max}	46 K	67 K
Temperature range for S_r > 1 %K^{-1}	16-117 K	-
Temperature uncertainty (δT)	0.001-0.009 K	0.09-0.1 K
SMM range	2-12 K	2-16 K
U_{eff} (cm^{-1})	50 K	173 K
S_r in SMM range	0.7-1.13 % K^{-1}	0.46-0.58 % K^{-1}
Average lifetime (at 10K)	1.92 ns	5.53 ns

Discussion on the improved thermometric performance of 1Np over 1Ph:

The enhanced thermometry performance of 1Np compared to 1Ph is primarily supported by three key factors: denser crystal packing, a faster-excited state lifetime decay of Dy, and a smaller energy gap between S_1 and $^4F_{9/2}$ in 1Np compared to 1Ph.

a) Denser crystal packing in 1Np will reduce the vibrational relaxation compared to 1Ph, thereby enhancing energy transfer efficiency from ligand donor states to the metal acceptor levels: increasing photosensitization in 1Np.

b) Due to the more conjugated nature, the energy levels of 1Np are lower compared to 1Ph. Thus, the energy gap between ligand S_1 and metal $^4F_{9/2}$ is lesser in 1Np. Hence the energy transfer from ligand S_1 to metal acceptor level will be more efficient as well as faster in 1Np and eventually it will relax faster compared to 1Ph. Hence, we observed a faster and lower value of average lifetime for 1Np compared to 1Ph. Thus, the faster-excited state lifetime decay also indicates an efficient energy sensitization happening in 1Np.

All the above-mentioned factors lead to enhanced photosensitization in 1Np compared to 1Ph. This is reflected in the emission intensity, as 1Np exhibits very high emission intensity compared to 1Ph throughout the temperature range of 10-300 K (Figure S11). This increased luminescence intensity improves the signal-to-noise ratio (SNR), which is critical for accurate temperature measurements. A

higher SNR in 1Np allows for more precise detection of subtle changes in the luminescent signal, which is important for achieving high-resolution thermometry.[6]

Table S6: A comparative table of magnetic and photophysical parameters for complexes 1Np and 1Ph with other reported Dy(III) luminescent thermometers.

Dy(III) Luminescence Thermometers	U_{eff} (K)	ΔT (K)	S_m (% K^{-1})	T_m (K)	References
$[Dy_2(bpm)(tfac)_6]$	-	5.4-85.5 90-300 300-398	1.8 0.5 3.3	5.4 90 298	ACS Cent. Sci., **2019**, 5 , 1187—1198
$[Dy(acac)_3(PyAm)]$	137	12-323	2	12	Chem. Commun., **2021**, 57, 7818—7821
[Dy(bbpen)Cl]	942	12-300	0.3	255	Angew. Chem., Int. Ed., **2023**, 62 , e202306970
$[Dy(acac)_3(bpm)]$	309	30-140	1.5	70	Chem. Commun., **2023**, 59, 8723—8726
$Dy_2(Np)_6(bpym)$ **$Dy_2(Ph)_6(bpym)$**	50.00 173.18	10-300 10-300	1.60 0.97	46 67	**Our work**

S9. References

[1] G. Sheldrick, *Acta Crystallographica Section A* **2015**, *71*, 3-8.

[2] O. V. Dolomanov, L. J. Bourhis, R. J. Gildea, J. A. K. Howard, H. Puschmann, *Journal of Applied Crystallography* **2009**, *42*, 339-341.

[3] G. Sheldrick, *Acta Crystallographica Section C* **2015**, *71*, 3-8.

[4] P. Hu, M. Ding, X. Gao, A. Zhu, F. Xiao, J. Cao, Y. Zhang, *Cryst. Eng. Comm.* **2024**, *26*, 4657-4668.

[5] A. G. Bispo-Jr, L. Yeh, D. Errulat, D. A. Gálico, F. A. Sigoli, M. Murugesu, *Chem. Commun.* **2023**, *59*, 8723-8726.

[6] aC. D. S. Brites, R. Marin, M. Suta, A. N. Carneiro Neto, E. Ximendes, D. Jaque, L. D. Carlos, *Advanced Materials* **2023**, *35*, 2302749; bR. Vieira Perrella, G. Derroso, P. C. de Sousa Filho, *ACS Omega* **2024**, *9*, 34974-34980.